iScience

CellPress
OPEN ACCESS

Article

RSU-1 regulates the integrity of dense bodies in muscle cells of aging *Caenorhabditis elegans*

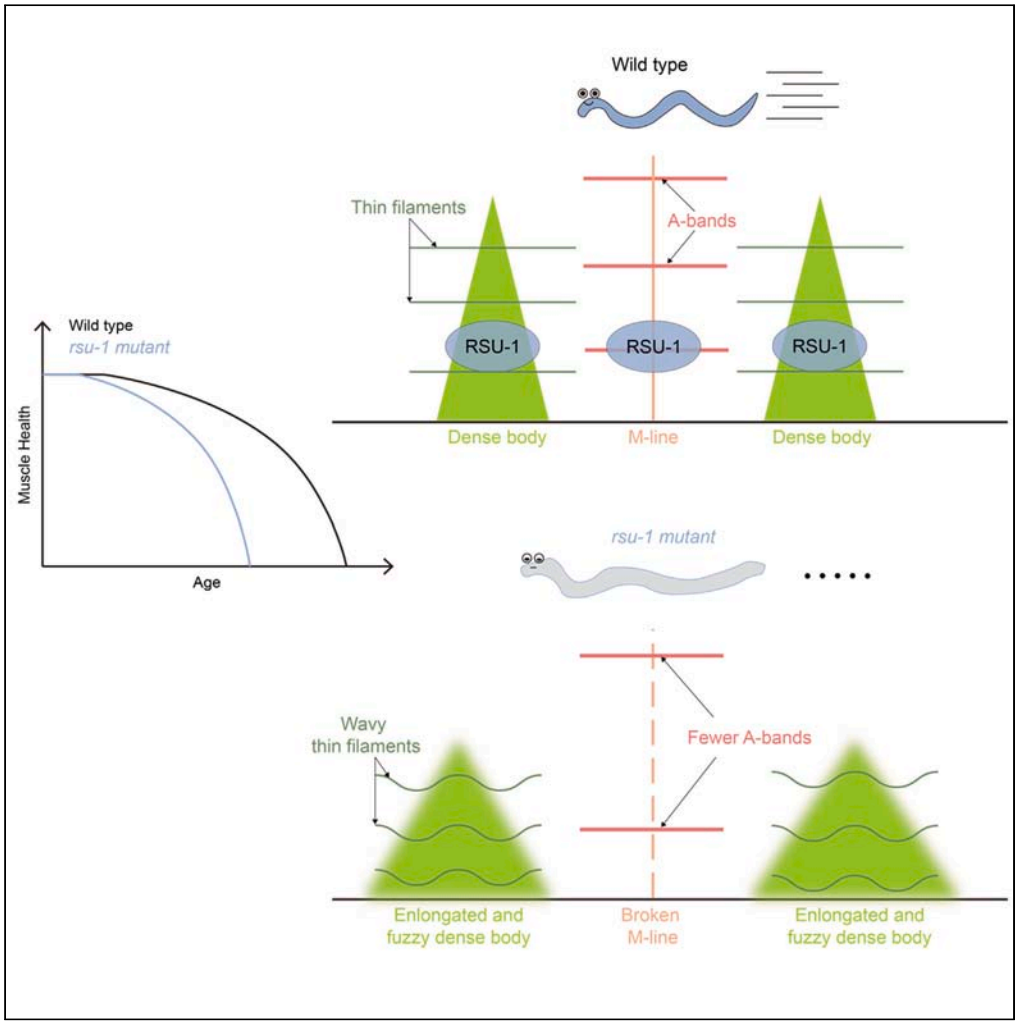

Ling Jiang, Xinyan Wang, Dandan Zhang, Karen Wing Yee Yuen, Yu Chung Tse

kwyyuen@hku.hk (K.W.Y.Y.)
tseyc@sustech.edu.cn (Y.C.T.)

Highlights

RSU-1 localizes at the ring-shaped dense body

RSU-1 maintains muscle integrity in aging *C. elegans*

The dense body and M-line structure vary across *C. elegans* body regions

RSU-1 and UNC-97 interaction is crucial for dense body structure in aging *C. elegans*

Jiang et al., iScience 27, 109854
June 21, 2024
https://doi.org/10.1016/j.isci.2024.109854

iScience

CellPress
OPEN ACCESS

Article

RSU-1 regulates the integrity of dense bodies in muscle cells of aging *Caenorhabditis elegans*

Ling Jiang,[1,2] Xinyan Wang,[3] Dandan Zhang,[2] Karen Wing Yee Yuen,[1,4,*] and Yu Chung Tse[2,3,5,*]

SUMMARY

Muscle contraction is vital for animal survival, and the sarcomere is the fundamental unit for this process. However, the functions of many conserved sarcomere proteins remain unknown, as their mutants do not exhibit obvious defects. To address this, *Caenorhabditis elegans* was utilized as a model organism to investigate RSU-1 function in the body wall muscle. RSU-1 is found to colocalize with UNC-97 at the dense body and M-line, and it is particularly crucial for regulating locomotion in aging worms, rather than in young worms. This suggests that RSU-1 has a specific function in maintaining muscle function during aging. Furthermore, the interaction between RSU-1 and UNC-97/PINCH is essential for RSU-1 to modulate locomotion, preserve filament structure, and sustain the M-line and dense body throughout aging. Overall, these findings highlight the significant contribution of RSU-1, through its interaction with UNC-97, in maintaining proper muscle cell function in aging worms.

INTRODUCTION

Muscle contraction plays a fundamental role in animal locomotion, allowing organisms to get food, evade predators, and locate suitable environments for reproduction and shelter. The sarcomere, functioning as the structural unit of striated muscle, governs muscle contraction and encompasses various components, including Z-disks, M-lines, thin filaments (actin), and thick filaments (myosin).[1,2] These sarcomeric constituents possess distinct functions and architectures that necessitate precise coordination. In *C. elegans* body wall muscle, a type of striated muscle, the Z-disk analogs are called the dense bodies. Dense bodies are located at the ends of thin filaments, whereas M-lines are positioned at the center of sarcomere.[3] As myosin filaments slide alongside actin filaments, mechanical force is transmitted from the muscle cell membrane to the basal lamina through the dense bodies and M-lines, thereby regulating muscle cell contraction and relaxation.[4] This precise coordination enables animals to achieve efficient locomotion. Consequently, any deviations in sarcomere assembly and contraction can lead to various muscular diseases, including muscular dystrophy and myofibrillar myopathies.[5]

On the other hand, as animals age, there is a gradual decline in their muscle mass, strength, and function, resulting in a condition known as sarcopenia.[6,7] Although the factors contributing to sarcopenia have been investigated from various aspects, including alterations in muscle protein synthesis, mitochondrial function, and inflammation,[8] there has been limited exploration of the structural changes in Z-disks and M-lines associated with sarcopenia.

The molecular components of dense bodies and M-lines are highly conserved among metazoans.[2,9] The nematode *Caenorhabditis elegans* (*C. elegans*) is a well-established model organism for the study of muscle architecture and development. In *C. elegans*, dense bodies represent electron-dense structures composed of cytoskeletal adaptor proteins, including UNC-52/perlecan, PAT-2/integrin α, PAT-3/integrin β, UNC-112/kindlin, PAT-4/integrin linked kinase, PAT-6/actopaxin, UNC-97/PINCH, DEB-1/vinculin, and ATN-1/α-actinin. These proteins facilitate the connection between the cytoplasmic domain of integrin and actin filaments.[9] In contrast to the dense body, the M-lines share the same membrane-proximal adaptors but have different membrane-distal proteins. Notably, the M-lines lack DEB-1/vinculin and ATN-1/α-actinin. Instead, M-line-specific proteins include UNC-82, UNC-89/obscurin, UNC-96, and UNC-98.[10–12]

In addition to the core proteins responsible for assembling the dense body and M-line, prior studies, as well as our finding, have indicated the presence of Ras suppressor (RSU-1) localization at the dense body and M-line in *C. elegans* muscle cells.[13] RSU-1 is well-conserved across metazoans. In human cultured cells, RSU-1 constitutes an important component of the focal adhesion complex. It binds to the LIM5 domain of UNC-97/PINCH, thereby stabilizing the complex and regulating cell adhesion and spreading.[14,15] Conversely, in human cells, RSU-1 has the ability to induce p38 Map Kinase phosphorylation independently of PINCH binding.[16] In addition, *C. elegans* RSU-1 promotes actin-bundle

[1]School of Biological Sciences, The University of Hong Kong, Kadoorie Biological Sciences Building, Pokfulam Road, Hong Kong, China
[2]School of Life Sciences, Department of Biology, Southern University of Science and Technology, Shenzhen 518055, China
[3]Core Research Facilities, Southern University of Science and Technology, Shenzhen 518055, China
[4]School of Biological Sciences, University of Southampton, Life Sciences Building (Building 85), Highfield Campus, Southampton SO17 1BJ, UK
[5]Lead contact
*Correspondence: kwyyuen@hku.hk (K.W.Y.Y.), tseyc@sustech.edu.cn (Y.C.T.)
https://doi.org/10.1016/j.isci.2024.109854

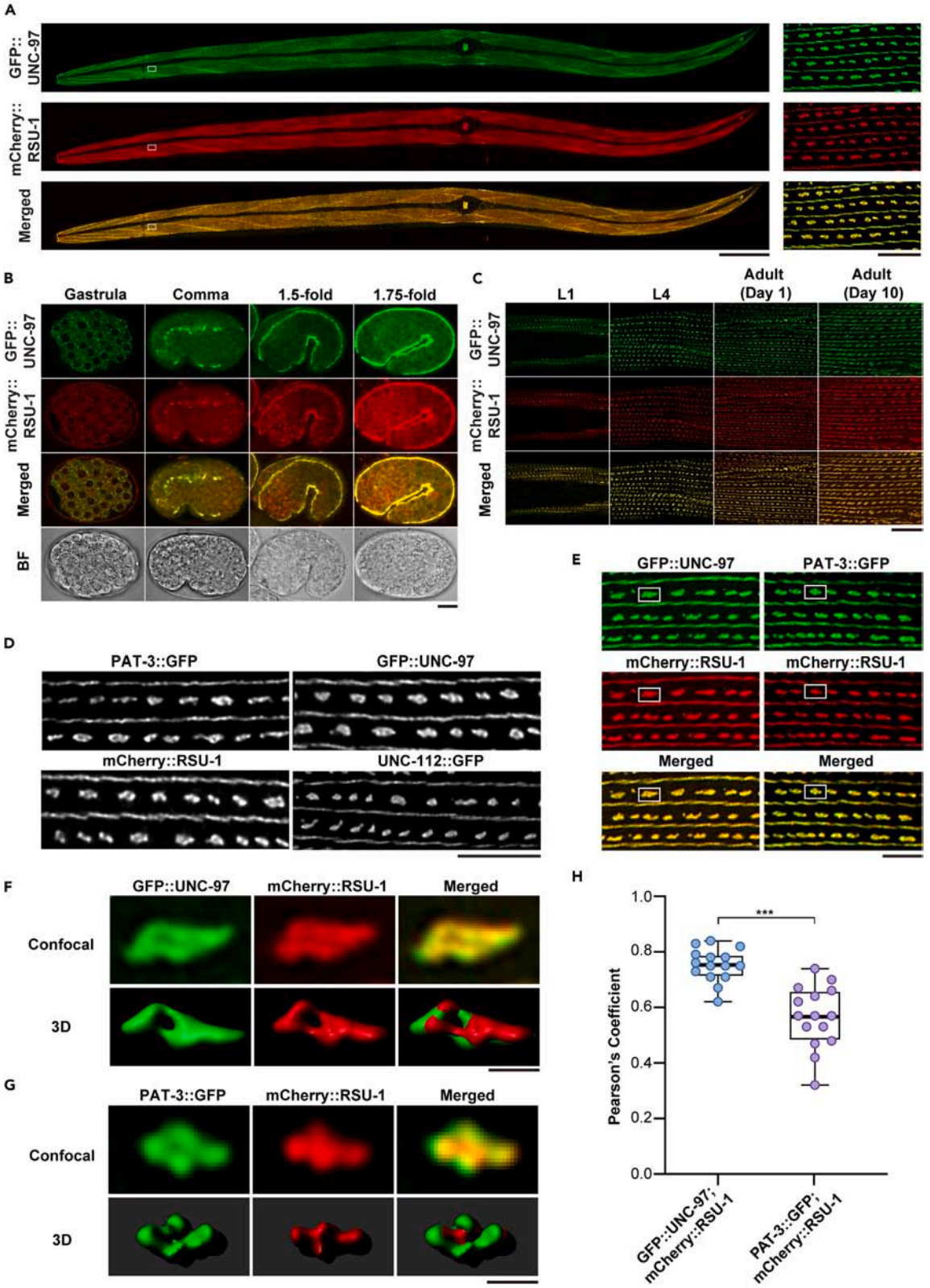
A
GFP::UNC-97
mCherry::RSU-1
Merged
B
Gastrula
Comma
1.5-fold
1.75-fold
GFP::UNC-97
mCherry::RSU-1
Merged
BF
C
L1
L4
Adult (Day 1)
Adult (Day 10)
GFP::UNC-97
mCherry::RSU-1
Merged
D
PAT-3::GFP
GFP::UNC-97
mCherry::RSU-1
UNC-112::GFP
E
GFP::UNC-97
PAT-3::GFP
mCherry::RSU-1
mCherry::RSU-1
Merged
Merged
F
GFP::UNC-97
mCherry::RSU-1
Merged
Confocal
3D
G
PAT-3::GFP
mCherry::RSU-1
Merged
Confocal
3D
H
Pearson's Coefficient
1.0
0.8
0.6
0.4
0.2
0.0
***
GFP::UNC-97; mCherry::RSU-1
PAT-3::GFP; mCherry::RSU-1

Figure 1. RSU-1 localizes in the ring-shaped dense body with UNC-97

(A) Representative confocal images illustrate the subcellular localization of GFP::UNC-97 and mCherry::RSU-1 in body wall muscle and vulval muscle. The right panel displays a zoomed-in image of the area enclosed by white box in the left panel. Scale bar, 100 μm in the left panel, 5 μm in the right panel.

(B and C) Representative confocal images show the subcellular localization of GFP::UNC- 97 and mCherry::RSU-1 at gastrula, comma, 1.5-fold, and 1.75-fold stages (B) and L1, L4, Day 1 adult, and Day 10 adult stages (C). Images in (B) are maximum intensity projections, whereas images in (C) are the single plane images. Scale bar, 10 μm.

(D) Representative high-resolution confocal images (resolution: 120 nm) exhibit the dense body in the four worm strains expressing PAT-3::GFP, mCherry::RSU-1, GFP::UNC-97, and UNC-112::GFP individually. Scale bar, 10 μm.

(E) Representative confocal images of strains coexpressing GFP::UNC-97 and mCherry::RSU-1 and PAT-3::GFP and mCherry::RSU-1. Scale bar, 5 μm.

(F and G) Constructed 3D images show the dense bodies marked by GFP::UNC-97 and mCherry::RSU-1 (F) and PAT-3::GFP and mCherry::RSU-1 (G) in the white box region from (E). The top plane displays the confocal images of a single dense body, whereas the bottom represents the simulated dense body based on the top plane. Scale bar, 0.5 μm.

(H) Comparison of the Pearson coefficients between GFP::UNC-97 and mCherry::RSU-1, as well as PAT-3::GFP and mCherry::RSU-1. Data were analyzed using unpaired Student's t test; *$p < 0.05$, **$p < 0.01$, ***$p < 0.001$; error bars, ±SEM.

organization in the vulval muscle,[17] and it is required for the proper distribution of extrasynaptic acetylcholine receptors (AChRs) in the muscle cells.[13] However, to date, there are a paucity of reports demonstrating the necessity of RSU-1 in body wall muscle contraction and development in *C. elegans*, and neither "Unc" (uncoordinated) nor "Pat" (paralyzed arrested at the 2-fold stage) phenotypes have been observed in *rsu-1* null mutants. Consequently, the reasons underlying the localization of RSU-1 at the dense body and M-line in muscle cells remain unclear.

In this study, we have demonstrated that RSU-1 is primarily expressed in the body wall muscle and colocalized with UNC-97/PINCH at the dense body. Additionally, our findings reveal that depletion of RSU-1 results in an earlier onset of sarcopenia in aging worms. Moreover, we have observed aggregation and distortion of actin and myosin filaments, as well as the enlargement and elongation of the dense body, in both the aging *rsu-1* null mutant and the *rsu-1* mutant with UNC-97 binding deficiency. Taken together, our results suggest that RSU-1 plays a crucial role in maintaining the structural integrity of the sarcomere in aging *C. elegans*, with its interaction with UNC-97 being crucial for this function. These findings contribute significantly to our understanding of the mechanisms underlying muscle function and aging, providing valuable insights for the development of novel therapeutic strategies targeting age-related muscle disorders.

RESULTS

RSU-1 colocalizes with UNC-97 at both dense bodies and M-lines

In our previous study, we reported the expression of RSU-1 in the vulval muscles of *C. elegans*, where it plays a regulatory role in α-actinin and contributes to the maintenance of vulval muscle integrity.[17] Additionally, in human cells, RSU-1 is known to localize to focal adhesions and interact with PINCH.[18] To elucidate the subcellular localization of RSU-1 in *C. elegans* muscle cells, we coexpressed mCherry::RSU-1 and GFP::UNC-97 by CRISPR/Cas9 genomic insertion and examined their subcellular localization. As expected, we observed colocalization of mCherry::RSU-1 and GFP::UNC-97 at the body wall muscle and vulva muscle in adult worms (Figure 1A).

Subsequently, we further investigated the expression pattern of RSU-1 throughout the life cycle of *C. elegans*. Our findings revealed that RSU-1 initially appeared in the cytosol of embryonic cells during early embryonic stages and gastrulation but progressively accumulated at body wall muscle attachments from the comma stage to the 2-fold stage (Figure 1B). Following hatching, RSU-1 localized to the M-lines, dense bodies, and adhesion sites of body wall muscle cells from L1 larval stage to the adult stage (Figure 1C). A notable observation is that the dense bodies, labeled by UNC-97 and RSU-1, exhibit a donut-shaped appearance rather than a solid dot in both Day 1 and Day 10 adults (Figure 1D). To investigate if this pattern is shared by other sarcomere proteins, GFP-tagged strains of PAT-3/integrin β and UNC-112/kindlin were utilized. Similarly, donut-shaped dense bodies were also observed, as depicted in Figure 1D.

To quantify the extent of colocalization between RSU-1 and the core proteins of the dense body, we coexpressed mCherry::RSU-1 with GFP::UNC-97 (CRISPR/Cas-9 genomic insertion) or mCherry::RSU-1 with PAT-3::GFP (extrachromosomal array) in worms and subsequently analyzed their colocalization coefficient within the dense body using high-resolution confocal microscopy (theoretical lateral resolution: 120 nm). Our findings revealed a high degree of colocalization between RSU-1 and UNC-97 within the dense body (Figures 1E and 1F), with a Pearson coefficient of 0.7527 ± 0.05958 (Figure 1H). However, we observed that the Pearson coefficient between RSU-1 and PAT-3 within the dense body (0.5660 ± 0.1126) is lower than RSU-1/UNC-97. In addition, RSU-1 and PAT-3 appeared to be intertwined with each other with different shapes (Figures 1E and 1G). These results indicate that RSU-1 is localized to the M-line and dense body of body wall muscle cells in *C. elegans* and is colocalized with UNC-97.

RSU-1 regulates locomotion ability in aging worms

After analyzing our results, which demonstrate that RSU-1 is located at the dense body of body wall muscle throughout the entire life cycle of *C. elegans*, we aimed to investigate the role of RSU-1 in maintaining dense body and M-line integrity and locomotion ability. To achieve this, we compared locomotion and burrowing ability among three groups: control worms, *rsu-1(RNAi)*-treated worms, and *rsu-1(tm6690)* mutant worms. The *rsu-1(tm6690)* mutant strain, obtained from NBRP, carries a 778 bp deletion at the N terminus of RSU-1 in the chromosome III, resulting in a presumed null deletion mutant (Figure 2B).[17] In these analyses, wild-type adult worms were bleached, and the embryos obtained

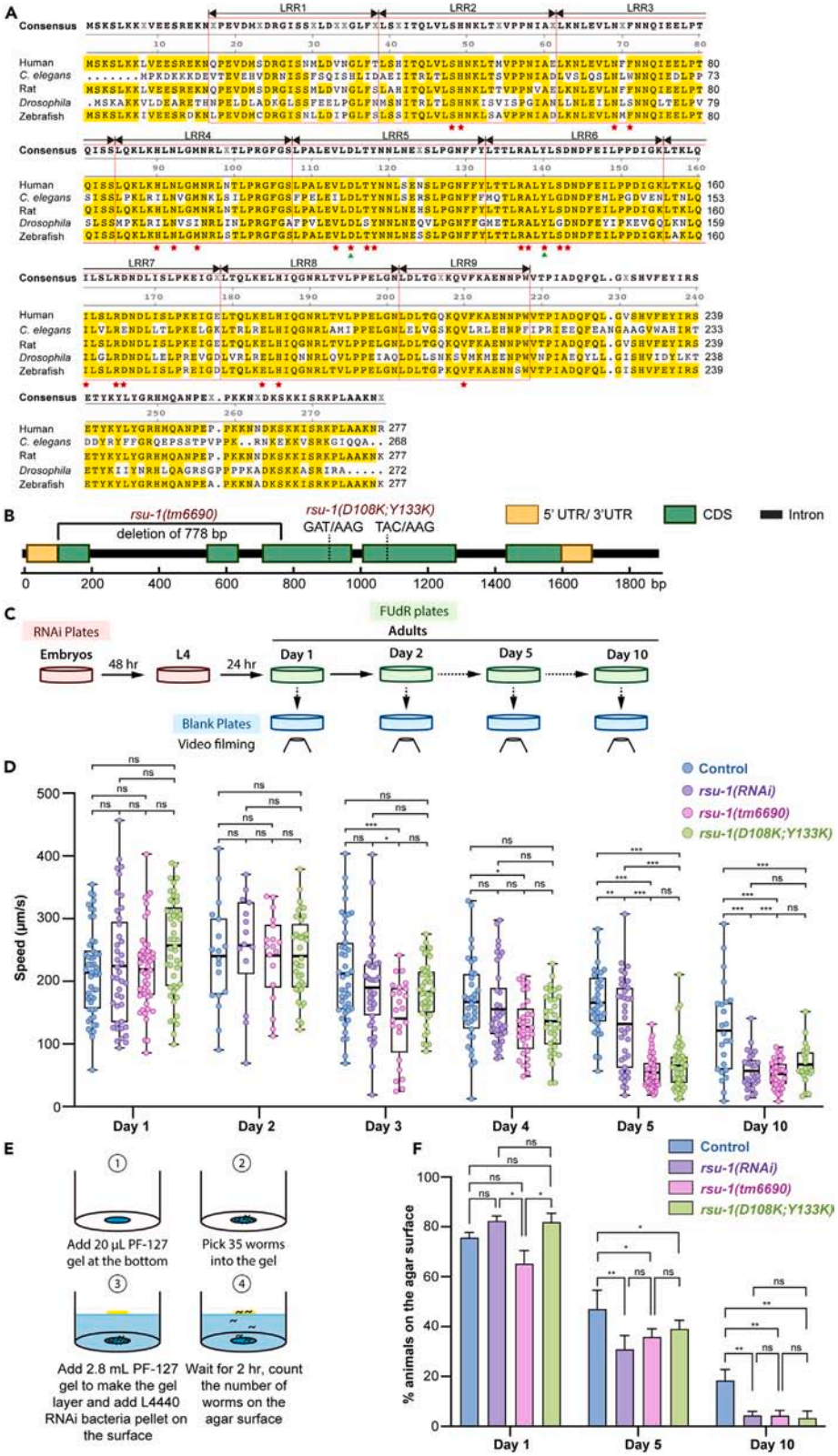
A
LRR1
LRR2
LRR3
Consensus
Human
C. elegans
Rat
Drosophila
Zebrafish
LRR4
LRR5
LRR6
LRR7
LRR8
LRR9
B
rsu-1(tm6690)
deletion of 778 bp
rsu-1(D108K;Y133K)
GAT/AAG TAC/AAG
5' UTR/ 3'UTR
CDS
Intron
C
RNAi Plates
Embryos
48 hr
L4
24 hr
FUdR plates
Adults
Day 1
Day 2
Day 5
Day 10
Blank Plates
Video filming
D
Control
rsu-1(RNAi)
rsu-1(tm6690)
rsu-1(D108K;Y133K)
Speed (μm/s)
Day 1
Day 2
Day 3
Day 4
Day 5
Day 10
E
Add 20 μL PF-127 gel at the bottom
Pick 35 worms into the gel
Add 2.8 mL PF-127 gel to make the gel layer and add L4440 RNAi bacteria pellet on the surface
Wait for 2 hr, count the number of worms on the agar surface
F
% animals on the agar surface

Figure 2. Loss of RSU-1 reduces the locomotion ability in the aging worms

(A) Amino acid sequence alignment of RSU-1 across different species performed with SnapGene software. Amino acids matching with the consensus are highlighted in yellow. Gray X indicates the variable amino acid. The conserved amino acids involving in UNC-97/PINCH interaction are indicated by the red stars. Double point mutant sites are highlighted by the green triangles.

(B) Schematic of the RSU-1 gene.

(C) Methodology of locomotion speed assay.

(D) Locomotion speed comparison among control, *rsu-1(RNAi)*, *rsu-1(tm6690)*, and *rsu-1(D108K;Y133K)* from Day 1 adults to Day 5 adults and Day 10 adults. Data were processed using WormLab software. Data were analyzed by unpaired Student's t test; $*p < 0.05$, $**p < 0.01$, $***p < 0.001$; error bars, ±SEM.

(E) Methodology of burrowing assay.

(F) Burrowing ability comparison among Day 1 adults, Day 5 adults, and Day 10 adults in control, *rsu-1(RNAi)*, *rsu-1(tm6690)*, and *rsu-1(D108K;Y133K)*. Three replicates were performed for each group.

were hatched on *L4440(RNAi)* plates or *rsu-1(RNAi)* plates, whereas *rsu-1(tm6690)* mutant embryos were only hatched on *L4440(RNAi)* plates. We then collected L4 worms and allowed them to grow on agar plates with 5-fluoro-2′-deoxyuridine (FUdR) to prevent egg production. Subsequently, we evaluated the speed of locomotion of Day 1 to Day 5 and Day 10 adult worms (Figure 2C).

Both control and *rsu-1(RNAi)*-treated worms exhibited a decline in locomotion speed at the Day 4 adult stage, which further decreased at the Day 10 adult stage. However, *rsu-1(tm6690)* mutant worms showed the decline starting from the Day 3 adult stage and reached the peak decrease at the Day 5 adults (Figure S1). Furthermore, at the Day 5 adult stage, *rsu-1(RNAi)*-treated worms and *rsu-1(tm6690)* mutant worms displayed a significant decrease in speed compared to control group. The difference became more pronounced at the Day 10 adult stage in the *rsu-1(RNAi)*-treated worms and *rsu-1(tm6690)* mutants (Figure 2D). To investigate the function of RSU-1 during the aging process, we selected Day 5 and Day 10 adults for further analysis.

Our findings reveal that all Day 1 young adult worms, including control worms, *rsu-1(RNAi)*-treated worms, and *rsu-1(tm6690)* mutant worms, displayed similar locomotion speeds: control (234.4 μm/s ± 83.72), *rsu-1(RNAi)*-treated worms (224.3 μm/s ± 94.90), and *rsu-1(tm6690)* mutant worms (206.4 μm/s ± 80.60) (Figure 2D). These results indicate that RSU-1 is not essential for the locomotion of young adults. Our observations align with previous studies that demonstrated the depletion of RSU-1 had no impact on the body wall muscle structure of young worms and the pharyngeal pumping rate.[17,19]

As the worms age, their locomotion speed significantly decreases.[20] Specifically, when compared to Day 1 control adult worms, the locomotion speed of Day 5 control adult worms declined by 29% (165.7 μm/s ± 51.22), and it dropped by 48% in Day 10 control adult worms (121.2 μm/s ± 73.48) (Figure 2D). Interestingly, the reduction in locomotion speed between young and old adult worms was even more pronounced in *rsu-1(RNAi)*-treated worms and *rsu-1(tm6690)* mutant worms. In comparison to Day 1 adult worms, the locomotion speed of *rsu-1(RNAi)*-treated worms decreased by 41% in Day 5 adult worms and 75% in Day 10 adult worms. For *rsu-1(tm6690)* mutant worms, it decreased by 73% and 75%, respectively (Figure 2D).

To further investigate the decline in movement ability resulting from the loss of RSU-1, we conducted a burrowing assay. We placed the worms at the bottom of the PF-127 gel and counted the number of worms that reached the surface of the gel after 2 h (Figure 2E). Our results indicated that 70%–80% of Day 1 control adult worms, *rsu-1(RNAi)*-treated worms, and *rsu-1(tm6690)* mutant worms successfully crawled to the surface with no significant difference between the groups. However, consistent with the results from the locomotion assay, the burrowing abilities of Day 5 and Day 10 *rsu-1(RNAi)*-treated worms and *rsu-1(tm6690)* mutant worms were significantly lower than those of control worms of the same ages (Figure 2F). Therefore, these findings provide evidence that RSU-1 is essential for maintaining locomotion ability in aging worms.

The interaction between RSU-1 and UNC-97 regulates the locomotion ability of aging worms

Considering the significant colocalization of RSU-1 and UNC-97 within the dense body (Figures 1E–1H) and known physical interaction between them in human cells,[21] we hypothesized that the interaction between RSU-1 and UNC-97 plays a critical role in maintaining proper locomotion in aging worms. The interaction between them has been extensively studied, and RSU-1 contains nine LRR domains that bind to PINCH and are highly conserved between metazoans. Within these conserved binding sites, it has been shown that specific double point mutations, D115K and Y140K in human cells, have been shown to decrease the binding affinity compared to wild-type protein.[18,21] By aligning the amino acid sequence of RSU-1 in humans and *C. elegans* (Figure 2A), we identified that the corresponding conserved amino acids in *C. elegans* are D108 and Y133.

To test this hypothesis, we generated a *rsu-1* mutant strain (*rsu-1(D108K;Y133K)*) using CRISPR Cas9 genomic mutation, introducing two-point mutations at residues 108 and 133 within the UNC-97-binding domain of RSU-1 (Figures 2A and 2B).[19,21] In addition, we created a mCherry tagged RSU-1(D108K; Y133K) strain through CRISPR Cas9 genomic insertion. Although RSU-1 exhibited clear localization at the dense body, M-line, and adhesion sites, RSU-1(D108K; Y133K) displayed diminished localization with irregular puncta in muscle cells (Figure S2). Consequently, the dense body and M-line became undistinguishable due to the low signal. These observations indicate that RSU-1(D108K;Y133K) fails to localize properly in the body wall muscle.

Our results demonstrated a significant reduction in both locomotion speed and the number of worms present on the gel surface during the burrowing assay in aging *rsu-1(D108K;Y133K)* mutant worms when compared to control worms (Figures 2D and 2F). Conversely, the locomotion and burrowing abilities of *rsu-1(D108K;Y133K)* mutant worms closely resembled those of *rsu-1(RNAi)*-treated worms and *rsu-1(tm6690)* mutant worms (Figures 2D and 2F). Thus, these results indicate that the interaction between RSU-1 and UNC-97 is indispensable for the normal locomotion and burrowing ability of aging worms, with no noticeable effect on young adult worms.

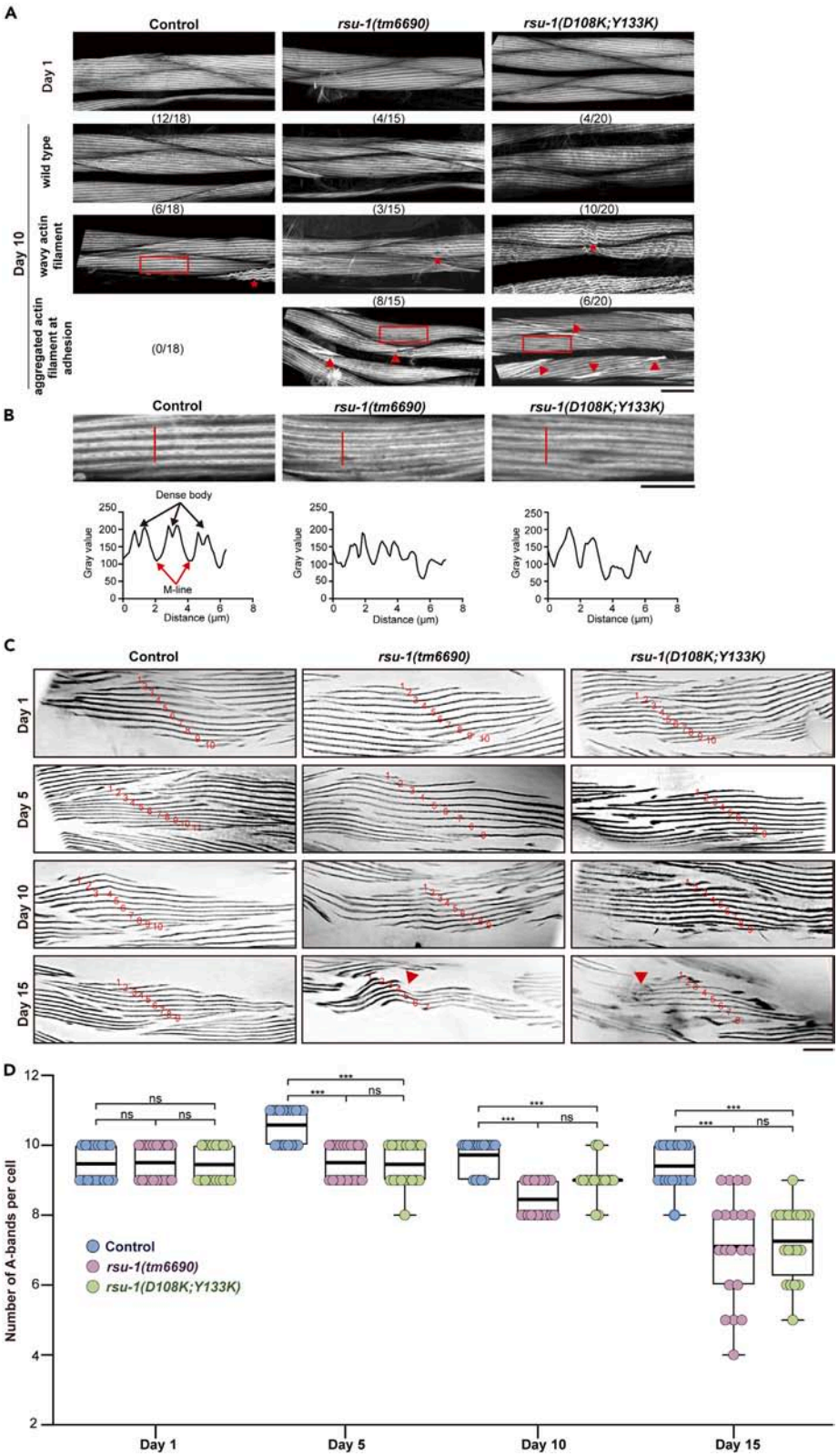
A
Control
rsu-1(tm6690)
rsu-1(D108K;Y133K)
Day 1
Day 10
wild type
wavy actin filament
aggregated actin filament at adhesion
(12/18)
(4/15)
(4/20)
(6/18)
(3/15)
(10/20)
(8/15)
(6/20)
(0/18)
B
Control
rsu-1(tm6690)
rsu-1(D108K;Y133K)
Dense body
M-line
Gray value
Distance (μm)
C
Control
rsu-1(tm6690)
rsu-1(D108K;Y133K)
Day 1
Day 5
Day 10
Day 15
D
Number of A-bands per cell
Control
rsu-1(tm6690)
rsu-1(D108K;Y133K)
ns
***
Day 1
Day 5
Day 10
Day 15

Figure 3. RSU-1 regulates the integrity of thin and thick filaments

(A) Representative confocal images depict phalloidin staining, marking actin filaments in Day 1 and 10 adult worms of control, *rsu-1(tm6690)*, and *rsu-1(D108K;Y133K)* mutants. Wavy F-actin filaments and F-actin aggregation are indicated by stars and arrowheads, respectively. Scale bar, 20 μm.

(B) Zoomed-in view of the red box in (A). The red line represents the region used for intensity line-scan analysis. Scale bar, 10 μm.

(C) Representative confocal images display A-bands immunostained with MHC A antibody in muscle cells at Day 1, 5, 10, and 15 adults. Red arrowhead indicates the disorganized wavy filament. Scale bar, 20 μm.

(D) Quantification of number of A-bands per muscle cell at different adulthood stages (Day 1, 5, 10, and 15 adults). Data were analyzed using unpaired Student's t test; *$p < 0.05$, **$p < 0.01$, ***$p < 0.001$; error bars, ±SEM.

RSU-1 regulates the integrity of thin and thick filaments in aging worms

Next, we further investigate the molecular mechanism on how RSU-1 regulates muscle contraction during aging. To achieve this, we examined the organization of sarcomeric actin and myosin in the absence of RSU-1 during aging. We employed rhodamine phalloidin staining to visualize actin thin filaments, as it specifically binds to filamentous actin.[3,22] Additionally, myosin thick filaments were observed through immunofluorescence using the Myosin A antibody, which is the central component of the thick filament.[23,24]

As shown in Figure 3A, neither the *rsu-1(tm6690)* mutant worms nor the *rsu-1(D108K;Y133K)* mutant worms showed any noticeable impact on the organization of actin filaments in Day 1 adult worms. However, by Day 10, there was an increased presence of wavy F-actin filaments in control worms (6/18), *rsu-1(tm6690)* mutant worms (3/15), and *rsu-1(D108K;Y133K)* mutant worms (10/20). Notably, the aggregation of F-actin filaments near the muscle cell boundaries was exclusively observed in *rsu-1(tm6690)* mutant worms (8/15) and *rsu-1(D108K;Y133K)* mutant worms (6/20). Additionally, actin striation, in control worms, appeared parallel and homogeneous, with a clear exclusion of signal from the dense body sites. However, both RSU-1 mutants showed a fuzzy actin striation where the dense bodies were undistinguishable and spaces between adjacent striations were irregular (Figure 3B), resembling the phenotypes induced by *lev-11(RNAi)*.[25,26] Thus, these results demonstrated that RSU-1 plays a crucial role in maintaining the proper organization of actin filaments within the muscle cells of aging worms.

Regarding the thick filaments, when comparing Day 1 adult worms of *rsu-1(tm6690)* mutant and *rsu-1(D108K;Y133K)* mutant to control adult worms, no appreciable alterations in the organization of thick filaments and number of A-bands were observed (Figures 3C and 3D). However, as the worms progressed to Day 5 and Day 10 of adulthood, a reduction in the number of A-bands in each muscle cell were observed in both *rsu-1(tm6690)* mutant worms and *rsu-1(D108K;Y133K)* mutant worms (Figures 3C and 3D). Additionally, atypical occurrences of disorganized wavy filaments were found in both Day 15 adult worms of the *rsu-1(tm6690)* mutant and *rsu-1(D108K;Y133K)* mutant. These results further substantiate the essential role of RSU-1 in regulating the organization of actomyosin networks within the muscle cells of aging worms.

RSU-1 maintains the integrity of dense bodies and M-lines in aging worms

As dense bodies and M-lines act as anchors for thin and think filaments, respectively, we conducted further investigations into whether RSU-1 regulates the structural integrity of these components within the body-wall muscle cells. High-resolution confocal microscopy was used to evaluate the structure of the dense body and M-line in transgenic worms expressing GFP::UNC-97 and mCherry::RSU-1. Our findings revealed region-specific characteristics of these components. In region 1 (head region), the dense bodies predominantly showed a round, donut-shaped appearance, whereas in region 4 (tail region), they appeared flattened (Figures 4A and 4B). To confirm our observation, we analyzed the oblate of dense body, as shown in Figure 4C. The oblate is a numerical parameter used to describe the shape of a spheroid, A smaller oblate suggests a more elongated or cigar-shaped spheroid. By quantifying the length and oblate of the dense body, the length increased from region 1 to region 4, whereas the oblate decreased from region 1 to 4 (Figure 4C). These findings further support our observation that the shape of the dense body changes from a more disk-shaped structure in region 1 to a more elongated or cigar-like structure in region 4.

Furthermore, significant differences in the structure of M-lines were observed among the head, middle, and tail regions. Regions 1 and 4 displayed zig-zagged M-lines, whereas regions 2 and 3 showed linear M-lines (Figures 4D and 4E). Additionally, dynamic changes in dense body organization were observed during the aging process. At Day 1, PAT-3 and RSU-1 showed considerable colocalization (Pearson correlation coefficient: 0.5961 ± 0.1082) (Figure S3A). However, from Day 5 to Day 15, there was progressive colocalization between PAT-3 and RSU-1 (Pearson correlation coefficient: Day 5—0.6311 ± 0.05290; Day 10—0.6578 ± 0.07032; Day 15—0.7470 ± 0.08849) (Figures S3B and S3C). These results indicate variations in dense body structure across different regions and aging stages.

To facilitate a comparative analysis, we further examined the structures of the dense bodies and M-lines in region 2 among control worms, *rsu-1(tm6690)* mutant worms, and *rsu-1(D108K;Y133K)* mutant worms at different ages (Day 1, 5, and 10). In control worms, the M-line consistently appeared linear and maintained a continuous intensity profile, with only a few gaps, across all three age groups (Figures 5A–5C). Similarly, the array of dense bodies in Day 1 control adult worms exhibited high organization, with uniform lengths (1.334μm ± 0.2132, Figures 5A and 5D). However, upon reaching Day 5 and Day 10, the length of dense bodies became variable and elongated (1.757μm ± 0.6637 and 1.963μm ± 0.5576, respectively) (Figure 5D). This dynamic elongation of the dense bodies may be correlated with the observed weakened locomotion ability in aging control worms (Figure 2D).

On the other hand, in Day 1 adult *rsu-1(tm6690)* mutant worms and Day 1 adult *rsu-1(D108K;Y133K)* mutant worms, the M-lines showed discontinuity with numerous gaps, and this pattern persisted in Day 5 and Day 10 adult worms (Figures 5A–5C). Furthermore, although both Day 1 *rsu-1* mutants had dense bodies of similar length to the control worms (Figure 5D), the dense bodies significantly elongated

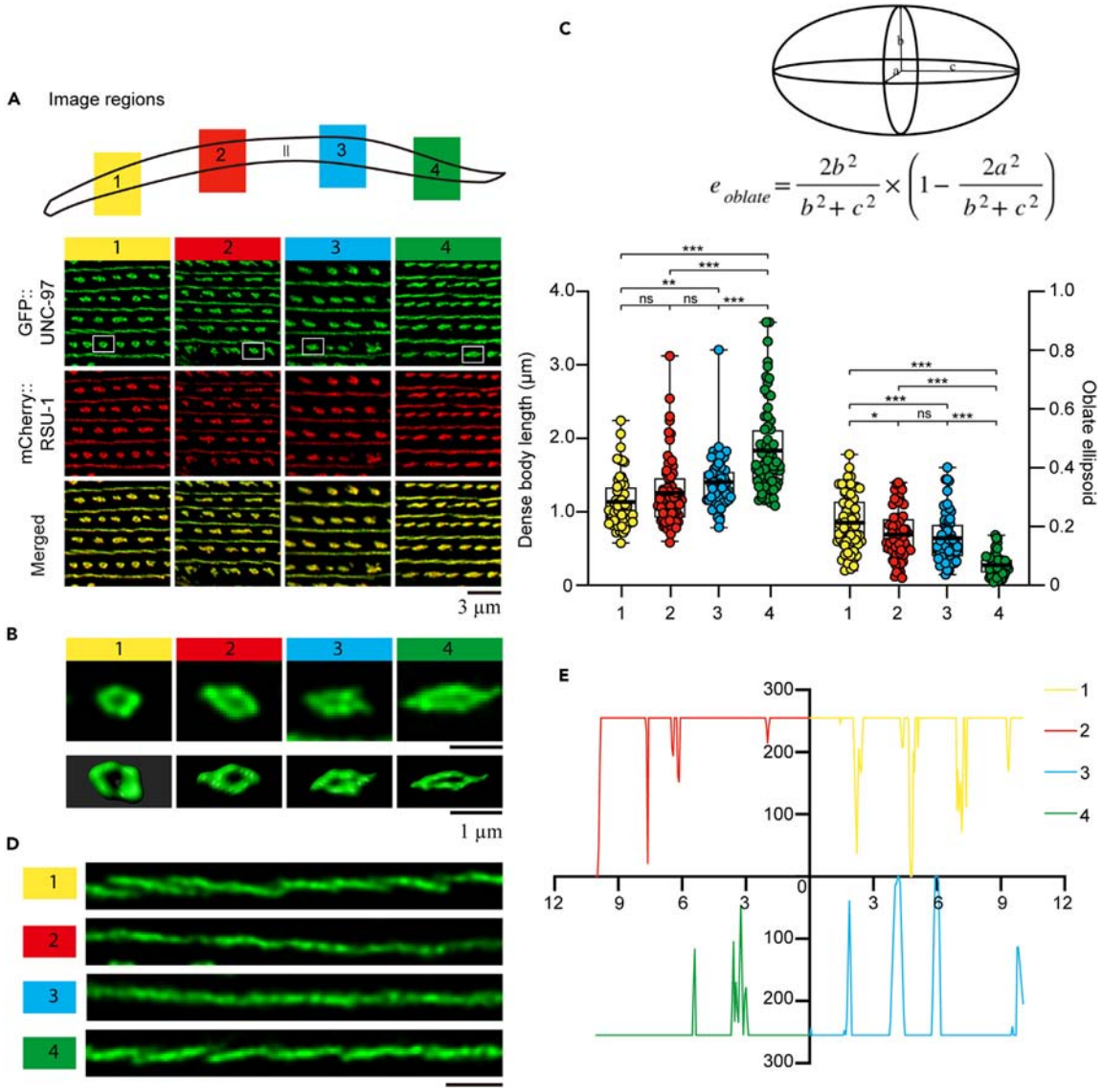

Figure 4. Variations in the structure of the dense body and M-line across different regions of the worms

(A) Representative confocal images illustrate the subcellular localization of GFP::UNC-97 and mCherry::RSU-1 in four regions across the entire worm, as depicted in the top plane. Scale bar, 3 μm.

(B) Representative confocal images of a single dense body from the white box in the (A), with the bottom plane showing the simulated dense body by Imaris software. Scale bar, 1 μm.

(C) Quantification of dense body length and oblate ellipsoid parameters in region 1, 2, 3, and 4 shown in the (A). Data were analyzed using unpaired Student's t test; *$p < 0.05$, **$p < 0.01$, ***$p < 0.001$; error bars, ±SEM.

(D) Representative confocal images display the M-lines in region 1, 2, 3, and 4. Scale bar, 20 μm.

(E) The continuity of the M-line in region 1, 2, 3, and 4.

at Day 5 (*rsu-1(tm6690)* mutant: 1.340μm ± 0.2100 [Day 1] to 3.463μm ± 1.728 (Day 5); *rsu-1(D108K;Y133K)* mutant: 1.347μm ± 0.4384 [Day 1] to 2.759μm ± 1.539 [Day 5]). Additionally, the pattern of dense bodies became irregular, and the lengths were varied significantly in both *rsu-1* mutant worms (Figure 5D).

To further investigate RSU-1 function in ultrastructure of dense bodies in *aging* worms, we conducted transmission electron microscopy imaging. In control, *rsu-1(tm6690)*, and *rsu-1(D108K;Y133K)* mutant worms, dense bodies were observed to be highly dense in Day 1 adult stage (Figure 5E). The TEM images confirmed alterations in the dense body of aging *rsu-1(tm6690)* and *rsu-1(D108K;Y133K)* mutants in Day 10 adult worms. In control worms, the dense bodies were highly condensed structures with well-defined edges (Figure 5F). However, in both Day 10 adult *rsu-1(tm6690)* and *rsu-1(D108K;Y133K)* mutant worms, the dense bodies appeared flattened, with less tightly defined

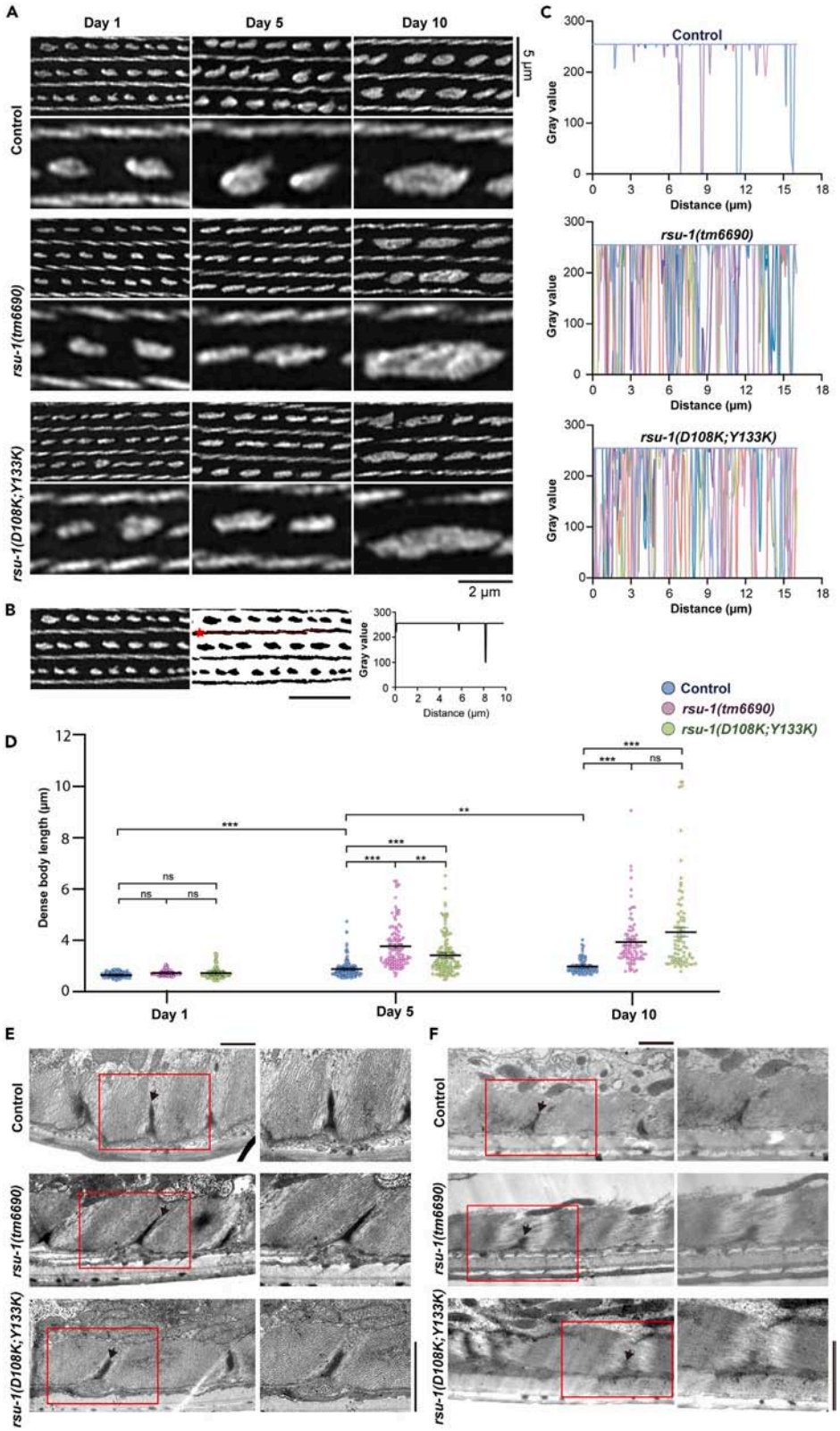
A
Day 1
Day 5
Day 10
Control
rsu-1(tm6690)
rsu-1(D108K;Y133K)
5 μm
2 μm
B
Gray value
Distance (μm)
C
Control
rsu-1(tm6690)
rsu-1(D108K;Y133K)
Gray value
Distance (μm)
D
Control
rsu-1(tm6690)
rsu-1(D108K;Y133K)
Dense body length (μm)
Day 1
Day 5
Day 10
ns
***
**
E
F
Control
rsu-1(tm6690)
rsu-1(D108K;Y133K)

Figure 5. RSU-1 maintains the structure of dense body in aging worms

(A) Representative confocal images of muscle region 2, as classified by Figure 4A, show GFP::UNC-97-labeled dense bodies and M-lines in Day 1, Day 5, and Day 10 adults worms of control, *rsu-1(tm6690)*, and *rsu-1(D108K;Y133K)* mutants. Scale bar, 5 μm for top row and 2 μm for bottom row.

(B) The continuity assessment of the M-line (indicated by the red star). The original image was converted to 8 bit, and the threshold was adjusted. The plot file of the segmented red line with a 1-pixel width (red ROI) was then applied. Scale bar, 5 μm.

(C) The continuity of the M-line in Day 10 worms of control, *rsu-1(tm6690)*, and *rsu-1(D108K;Y133K)* mutants. Each group comprises eight worms, and each differently colored line within the group represents the intensity of the M-line within muscle region 2 in different worms.

(D) Quantification of the dense body length in control, *rsu-1(RNAi)*, *rsu-1(tm6690)*, and *rsu-1(D108K;Y133K)* worms at Day 1, Day 5, and Day 10 adults, based on (A). The length of the dense body was measured using Imaris software. Data were analyzed using unpaired Student's t test; *$p < 0.05$, **$p < 0.01$, ***$p < 0.001$; Error bars, ±SEM.

(E and F) Representative TEM images of muscle region 2 show the dense body in Day 1 (E) and Day 10 (F) adults of control, *rsu-1(tm6690)*, and *rsu-1(D108K;Y133K)* mutants. Right panel displays a higher magnification of the region enclosed by red box in the left panel. Arrow indicates the dense body. Scale bar, 1 μm.

edges (Figure 5F). These results indicate that RSU-1 plays a crucial role in maintaining the integrity of dense bodies in aging worms, and this maintenance is dependent on the RSU-1-UNC-97 interaction.

DISCUSSION

As individuals age, they commonly experience sarcopenia, characterized by the decline of muscle mass and function. The precise mechanisms driving this process remain incompletely understood, but there is evidence to suggest that alterations in the structure and function of sarcomeres may contribute. This study provides valuable insights into the role of RSU-1 in maintaining the sarcomere integrity in aging *C. elegans*.

The dense bodies consist of several sarcomere proteins and function as the anchoring sites for thin filaments, forming densely packed structures within muscle cells. Traditional imaging techniques showed dense bodies as solid dot-like structures.[9,27] However, our high-resolution confocal imaging reveals a more intricate structure as the core components of the dense bodies are not closely colocalized with each other. PAT-3-marked donut-shaped structures intertwine with RSU-1 and UNC-97, potentially stabilizing dense body integrity. Importantly, the size and shape of dense bodies vary in different body regions, with circular shapes in the head region and flattened shapes in the tail region, suggesting deliberate structural variations for efficient force transmission during locomotion. The dense bodies are enlarged and elongated in aging mutants, and these aging mutants have much weaker locomotion abilities. Worms may require the proper size and shape of the dense body to optimize the efficiency of muscle contraction for locomotion. However, currently, there is no suitable method available to instantly monitor the structural changes of dense bodies at high resolutions during free worm movement.

It is important to note that the structure of the sarcomere observed under microscopes in many studies, including ours, reflects its relaxed stage when body wall muscles are treated with tetramisole to induce paralysis for imaging. Therefore, the correlation of sarcomere ultrastructure with locomotion assay data and burrowing assay data is commonly used to study the effect of sarcomere alterations on muscle integrity. Our results indicate that aging *rsu-1* mutants show decline in locomotion speed and burrowing ability (Figures 2D and 2F), accompanied by impaired focal adhesion stability (Figure 3A), distorted actomyosin networks (Figure 3C), and elongated dense bodies (Figures 5D and 5F). Additionally, a previous study demonstrated that RSU-1 maintains the stability of focal adhesions in MCF10A cells.[18] These findings provide evidence to support our hypothesis that RSU-1 contributes to the stability of focal adhesions at the cellular level and body wall muscle integrity at the organism level, thereby affecting aging worms (Figure 6).

Aging involves physical and biological dysfunction, including reduced motility, muscle degeneration, and impaired learning ability.[28,29] Muscle function decline is a common feature observed in both *C. elegans* and humans, manifested as reduced locomotion, decreased muscle mass, and disorganized myofilaments including the nervous system deterioration and body wall muscle degeneration.[7,30,31] Although the nervous system appears well maintained during aging, attention has shifted toward muscle structure alteration during aging.[32,33] In this study, we demonstrated locomotion decline and sarcomere disorganization during aging in worms. Loss of RSU-1 or the absence of the RSU-1-PINCH interaction accelerated the onset of sarcopenia in *C. elegans*. Additionally, gene transcription levels in different tissues undergo modifications during aging,[34,35] with declined expression of UNC-45, myosin, and HSP-90.[36] Yidong Shen's laboratory revealed that the expression level of RSU-1 is significantly lower in the intestine, but remain in muscle, hypodermis, and coelomocytes of Day 8 adult worms compared to the Day 1 adults.[34] Similar results were also obtained in our qPCR analysis, where the RSU-1 mRNA levels showed no significant difference between Day 1, Day 5, and Day 10 adult worms (Figure S4). To further investigate the mechanisms underlying RSU-1 regulation during aging, it would be beneficial to examine the RSU-1 protein levels and explore potential post-translational modifications, such as phosphorylation and degradation.

In conclusion, our study highlights the importance of RSU-1 and its interaction with UNC-97 in maintaining dense body and M-line integrity, supporting mobility during aging. These findings prompt a reevaluation of sarcomere proteins that show no visible phenotypes in young adult mutants, enhancing our understanding of sarcomere assembly, maintenance, and degradation during aging.

Limitations of the study

In this study, we conducted a comparative analysis of locomotion ability and sarcomere structure between wild-type worms and *rsu-1* mutants during the aging process. Our findings revealed the crucial role of RSU-1, a highly conserved protein across species, in maintaining the function and structure of the body wall muscle, which is relevant to sarcopenia. Additionally, we identified the significance of the interaction between RSU-1 and UNC-97 for the proper functioning of RSU-1. However, further investigations are warranted to elucidate the underlying

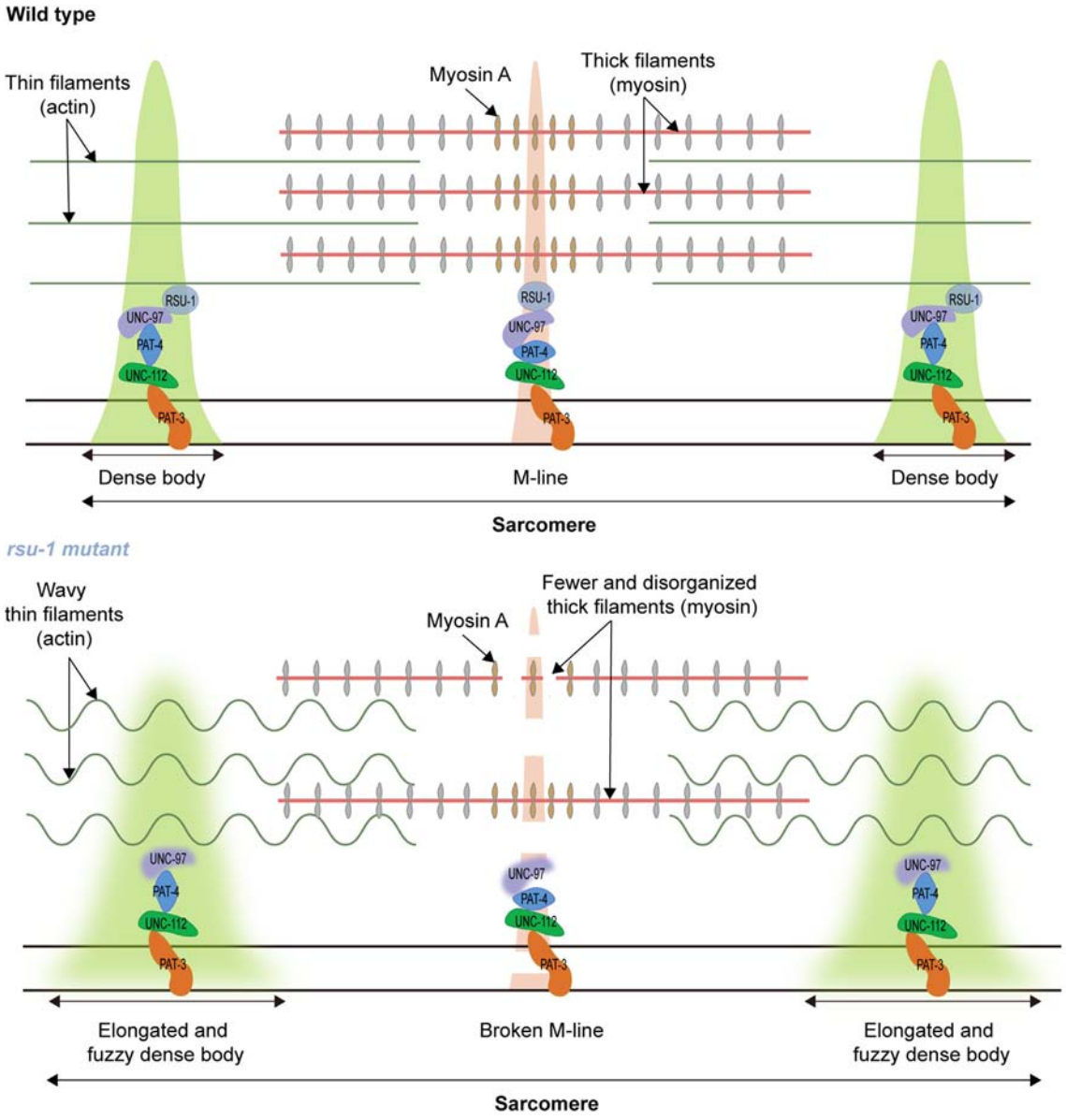

Figure 6. Simplified model of RSU-1 functions in the sarcomere structure during aging

The cartoon exhibits that RSU-1 (light blue) interacts with UNC-97 (purple) within dense body and M-line. The dense body (light green) and M-lines (orange) act as anchors for thin (green) and think filaments (red), respectively. Upon loss of RSU-1 in aging worms, UNC-97 (purple) is less intact within the dense body and M-line. Furthermore, the straight thin filaments become wavy with elongated and fuzzy dense bodies, and the number of A-bands are declined with disorganized thick filament and broken M-line.

mechanisms governing the regulation of RSU-1 during the aging process. These future studies will provide valuable insights into the molecular pathways associated with RSU-1 and its involvement in age-related muscle deterioration.

STAR★METHODS

Detailed methods are provided in the online version of this paper and include the following:

- KEY RESOURCES TABLE
- RESOURCE AVAILABILITY
  - Lead contact
  - Materials availability

SUPPLEMENTAL INFORMATION

Supplemental information can be found online at https://doi.org/10.1016/j.isci.2024.109854.

ACKNOWLEDGMENTS

We gratefully acknowledge the support of the SUSTech Core Research Facilities and HKU Center for PanorOmic Sciences (CPOS) for providing equipment for this study. Financial support for this research was provided by the National Natural Science Foundation of China (Grant No. 31671409) and Natural Science Foundation of Guangdong Province of China (Grant No. 2020A1515010742) to YCT.

AUTHOR CONTRIBUTIONS

Conceptualization and methodology: L.J., X.W., and Y.C.T.; investigation, analysis and writing: L.J. and Y.C.T.; resources and discussion: L.J., X.W., D.Z., K.W.Y.Y., and Y.C.T.; supervision: K.W.Y.Y. and Y.C.T.

DECLARATION OF INTERESTS

The authors declare no competing interests.

Received: December 8, 2023
Revised: March 19, 2024
Accepted: April 26, 2024
Published: April 30, 2024

REFERENCES

1. Sweeney, H.L., and Hammers, D.W. (2018). Muscle Contraction. Cold Spring Harb. Perspect. Biol. *10*, a023200. https://doi.org/10.1101/cshperspect.a023200.
2. Gieseler, K., Qadota, H., and Benian, G.M. (2017). Development, structure, and maintenance of C. elegans body wall muscle, *2017* (WormBook), pp. 1–59. https://doi.org/10.1895/wormbook.1.81.2.
3. Francis, G.R., and Waterston, R.H. (1985). Muscle organization in Caenorhabditis elegans: localization of proteins implicated in thin filament attachment and I-band organization. J. Cell Biol. *101*, 1532–1549. https://doi.org/10.1083/jcb.101.4.1532.
4. Lecuit, T., Lenne, P.F., and Munro, E. (2011). Force generation, transmission, and integration during cell and tissue morphogenesis. Annu. Rev. Cell Dev. Biol. *27*, 157–184. https://doi.org/10.1146/annurev-cellbio-100109-104027.
5. Lecroisey, C., Ségalat, L., and Gieseler, K. (2007). The C. elegans dense body: anchoring and signaling structure of the muscle. J. Muscle Res. Cell Motil. *28*, 79–87. https://doi.org/10.1007/s10974-007-9104-y.
6. Hosam, K., Kamel, M.D., FACN, FACP, and AGSF. (2003). Sarcopenia and Aging. Nutr. Rev. *61*, 157–167. https://doi.org/10.1301/nr.2003.may.
7. Janssens, G.E., Grevendonk, L., Perez, R.Z., Schomakers, B.V., de Vogel-van den Bosch, J., Geurts, J.M.W., van Weeghel, M., Schrauwen, P., Houtkooper, R.H., and Hoeks, J. (2022). Healthy aging and muscle function are positively associated with NAD+ abundance in humans. Nat. Aging *2*, 254–263. https://doi.org/10.1038/s43587-022-00174-3.
8. Wu, J., Ding, P., Wu, H., Yang, P., Guo, H., Tian, Y., Meng, L., and Zhao, Q. (2023). Sarcopenia: Molecular regulatory network for loss of muscle mass and function. Front. Nutr. *10*, 1037200. https://doi.org/10.3389/fnut.2023.1037200.
9. Moerman, D.G., and Williams, B.D. (2006). Sarcomere assembly in C. elegans muscle (WormBook), pp. 1–16. https://doi.org/10.1895/wormbook.1.81.1.
10. Benian, G.M., Tinley, T.L., Tang, X., and Borodovsky, M. (1996). The Caenorhabditis elegans gene unc-89, required fpr muscle M-line assembly, encodes a giant modular protein composed of Ig and signal transduction domains. J. Cell Biol. *132*, 835–848. https://doi.org/10.1083/jcb.132.5.835.
11. Qadota, H., Mayans, O., Matsunaga, Y., McMurry, J.L., Wilson, K.J., Kwon, G.E., Stanford, R., Deehan, K., Tinley, T.L., Ngwa, V.M., and Benian, G.M. (2016). The SH3 domain of UNC-89 (obscurin) interacts with paramyosin, a coiled-coil protein, in Caenorhabditis elegans muscle. Mol. Biol. Cell *27*, 1606–1620. https://doi.org/10.1091/mbc.E15-09-0675.
12. Miller, R.K., Qadota, H., Mercer, K.B., Gernert, K.M., and Benian, G.M. (2008). UNC-98 and UNC-96 interact with paramyosin to promote its incorporation into thick filaments of Caenorhabditis elegans. Mol. Biol. Cell *19*, 1529–1539. https://doi.org/10.1091/mbc.E07-07-0723.
13. Pierron, M., Pinan-Lucarré, B., and Bessereau, J.L. (2016). Preventing Illegitimate Extrasynaptic Acetylcholine Receptor Clustering Requires the RSU-1 Protein. J. Neurosci. *36*, 6525–6537. https://doi.org/10.1523/JNEUROSCI.3733-15.2016.
14. Wang, Z., Grange, M., Wagner, T., Kho, A.L., Gautel, M., and Raunser, S. (2021). The molecular basis for sarcomere organization in vertebrate skeletal muscle. Cell *184*, 2135–2150.e13. https://doi.org/10.1016/j.cell.2021.02.047.
15. Dougherty, G.W., Chopp, T., Qi, S.M., and Cutler, M.L. (2005). The Ras suppressor Rsu-1 binds to the LIM 5 domain of the adaptor protein PINCH1 and participates in adhesion-related functions. Exp. Cell Res.

306, 168–179. https://doi.org/10.1016/j.yexcr.2005.01.025.

16. Gonzalez-Nieves, R., DeSantis, A.I., and Cutler, M.L. (2013). Rsu1 contributes to regulation of cell adhesion and spreading by PINCH1-dependent and - independent mechanisms. J. Cell Commun. Signal. *7*, 279–293. https://doi.org/10.1007/s12079-013-0207-5.
17. Wang, X., Huang, S., Zheng, C., Ge, W., Wu, C., and Tse, Y.C. (2020). RSU-1 Maintains Integrity of *Caenorhabditis elegans* Vulval Muscles by Regulating α-Actinin. G3 (Bethesda) *10*, 2507–2517. https://doi.org/10.1534/g3.120.401185.
18. Fukuda, K., Lu, F., and Qin, J. (2021). Molecular basis for Ras suppressor-1 binding to PINCH-1 in focal adhesion assembly. J. Biol. Chem. *296*, 100685. https://doi.org/10.1016/j.jbc.2021.100685.
19. Izquierdo, P.G., Calahorro, F., Thisainathan, T., Atkins, J.H., Haszczyn, J., Lewis, C.J., Tattersall, J.E.H., Green, A.C., Holden-Dye, L., and O'Connor, V. (2022). Cholinergic signaling at the body wall neuromuscular junction distally inhibits feeding behavior in Caenorhabditis elegans. J. Biol. Chem. *298*, 101466. https://doi.org/10.1016/j.jbc.2021.101466.
20. Huang, C., Xiong, C., and Kornfeld, K. (2004). Measurements of age-related changes of physiological processes that predict lifespan of Caenorhabditis elegans. Proc. Natl. Acad. Sci. USA *101*, 8084–8089. https://doi.org/10.1073/pnas.0400848101.
21. Yang, H., Lin, L., Sun, K., Zhang, T., Chen, W., Li, L., Xie, Y., Wu, C., Wei, Z., and Yu, C. (2021). Complex structures of Rsu1 and PINCH1 reveal a regulatory mechanism of the ILK/PINCH/Parvin complex for F-actin dynamics. Elife *10*, e64395. https://doi.org/10.7554/eLife.64395.
22. Romani, M., and Auwerx, J. (2021). Phalloidin Staining of Actin Filaments for Visualization of Muscle Fibers in Caenorhabditis elegans. Bio. Protoc. *11*, e4183. https://doi.org/10.21769/BioProtoc.4183.
23. Qadota, H., Moody, J.C., Lesanpezeshki, L., Moncrief, T., Kitzler, D., Bhat, P.D., Vanapalli, S.A., Oberhauser, A.F., and Benian, G.M. (2020). A Region of UNC-89 (Obscurin) Lying between Two Protein Kinase Domains Is a Highly Elastic Spring Required for Proper Sarcomere Organization. J. Mol. Biol. *432*, 4799–4814. https://doi.org/10.1016/j.jmb.2020.06.024.
24. Miller, D.M., 3rd, Ortiz, I., Berliner, G.C., and Epstein, H.F. (1983). Differential Localization of Two Myosins within Nematode Thick Filaments. Cell *34*, 477–490.
25. Ono, S., Lewis, M., and Ono, K. (2022). Mutual dependence between tropomodulin and tropomyosin in the regulation of sarcomeric actin assembly in Caenorhabditis elegans striated muscle. Eur. J. Cell Biol. *101*, 151215. https://doi.org/10.1016/j.ejcb.2022.151215.
26. Gaiser, A.M., Kaiser, C.J.O., Haslbeck, V., and Richter, K. (2011). Downregulation of the Hsp90 system causes defects in muscle cells of Caenorhabditis elegans. PLoS One *6*, e25485. https://doi.org/10.1371/journal.pone.0025485.
27. Qadota, H., Matsunaga, Y., Nguyen, K.C.Q., Mattheyses, A., Hall, D.H., and Benian, G.M. (2017). High-resolution imaging of muscle attachment structures in Caenorhabditis elegans. Cytoskeleton (Hoboken) *74*, 426–442. https://doi.org/10.1002/cm.21410.
28. Lemoine, M. (2020). Defining aging. Biology & Philosophy *35*. Biol. Philos. *35*, 46. https://doi.org/10.1007/s10539-020-09765-z.
29. Lim, J.Y., and Frontera, W.R. (2022). Single skeletal muscle fiber mechanical properties: a muscle quality biomarker of human aging. Eur. J. Appl. Physiol. *122*, 1383–1395. https://doi.org/10.1007/s00421-022-04924-4.
30. Dridi, H., Forrester, F., Umanskaya, A., Xie, W., Reiken, S., Lacampagne, A., and Marks, A. (2022). Role of oxidation of excitation-contraction coupling machinery in age-dependent loss of muscle function in Caenorhabditis elegans. Elife *11*, e75529. https://doi.org/10.7554/eLife.75529.
31. Zhang, S., Li, F., Zhou, T., Wang, G., and Li, Z. (2020). Caenorhabditis elegans as a Useful Model for Studying Aging Mutations. Front. Endocrinol. *11*, 554994. https://doi.org/10.3389/fendo.2020.554994.
32. Herndon, L.A., Schmeissner, P.J., Dudaronek, J.M., Brown, P.A., Listner, K.M., Sakano, Y., Paupard, M.C., Hall, D.H., and Driscoll, M. (2002). Stochastic and genetic factors influence tissue-specific decline in ageing C. elegans. Nature *419*, 808–814. https://doi.org/10.1038/nature01135.
33. Garcia, G., Homentcovschi, S., Kelet, N., and Higuchi-Sanabria, R. (2022). Imaging of Actin Cytoskeletal Integrity During Aging in C. elegans. Methods Mol. Biol. *2364*, 101–137. https://doi.org/10.1007/978-1-0716-1661-1_5.
34. Wang, X., Jiang, Q., Song, Y., He, Z., Zhang, H., Song, M., Zhang, X., Dai, Y., Karalay, O., Dieterich, C., et al. (2022). Ageing induces tissue-specific transcriptomic changes in Caenorhabditis elegans. EMBO J. *41*, e109633. https://doi.org/10.15252/embj.2021109633.
35. Yu, G., Wu, Q., Gao, Y., Chen, M., and Yang, M. (2019). The Epigenetics of Aging in Invertebrates. Int. J. Mol. Sci. *20*, 4535. https://doi.org/10.3390/ijms20184535.
36. Matheny, C.J., Qadota, H., Kimelman, M., Bailey, A.O., Oberhauser, A.F., and Benian, G.M. (2022). UNC-45 Has a Crucial Role in Maintaining Muscle Sarcomeres during Aging in Caenorhabditis elegans. https://doi.org/10.1101/2022.06.04.494828.
37. Timmons, L., and Fire, A. (1998). Specific interference by ingested dsRNA. Nature *395*, 854. https://doi.org/10.1038/27579.
38. Sutphin, G.L., and Kaeberlein, M. (2009). Measuring Caenorhabditis elegans life span on solid media. J. Vis. Exp. 1152. https://doi.org/10.3791/1152.
39. Yin, J.A., Gao, G., Liu, X.J., Hao, Z.Q., Li, K., Kang, X.L., Li, H., Shan, Y.H., Hu, W.L., Li, H.P., and Cai, S.Q. (2017). Genetic variation in glia-neuron signalling modulates ageing rate. Nature *551*, 198–203. https://doi.org/10.1038/nature24463.
40. Lesanpezeshki, L., Hewitt, J.E., Laranjeiro, R., Antebi, A., Driscoll, M., Szewczyk, N.J., Blawzdziewicz, J., Lacerda, C.M.R., and Vanapalli, S.A. (2019). Pluronic gel-based burrowing assay for rapid assessment of neuromuscular health in C. elegans. Sci. Rep. *9*, 15246. https://doi.org/10.1038/s41598-019-51608-9.
41. Wilson, K.J., Qadota, H., and Benian, G.M. (2012). Immunofluorescent localization of proteins in Caenorhabditis elegans muscle. Methods Mol. Biol. *798*, 171–181. https://doi.org/10.1007/978-1-61779-343-1_10.
42. Ly, K., Reid, S.J., and Snell, R.G. (2015). Rapid RNA analysis of individual Caenorhabditis elegans. MethodsX *2*, 59–63. https://doi.org/10.1016/j.mex.2015.02.002.

STAR★METHODS

KEY RESOURCES TABLE

REAGENT or RESOURCE	SOURCE	IDENTIFIER
Bacterial and virus strains		
Escherichia coli OP50	Caenorhabditis Genetics Center	WBStrain00041969; RRID: WB-STRAIN:WBStrain00041969
Escherichia coli HT115	Ahringer's RNAi library	WBStrain00041079; RRID: WB-STRAIN:WBStrain00041079
Experimental models: Organisms/strains		
C. elegans	See Table S1 for details	N/A
Oligonucleotides		
Primers	See Table S2 for details	N/A
Antibodies		
Anti-MHC A (Mouse Monoclonal)	DSHB	Cat# 5-6; RRID: AB_2147425
Goat anti-mouse IgG-Alexa FluorTM Plus 647	ThermoFisher	Cat# A32728; RRID: AB_2866490
Chemicals, peptides, and recombinant proteins		
FUdR (5-Fluoro-2'-deoxyuridine)	ThermoFisher	40690016-2
Pluronic F-127	Beyotime	ST501-100g
(-)-Tetramisole	ApexBio	B1777
Paraformaldehyde	Electron Microscopy Sciences	15710-S
Rhodamine Phalloidin	Abcam	Cat# ab235138; RRID: AB_2572408
Software and algorithms		
GraphPad Prism9	Graphpad	https://www.graphpad.com/
ImageJ	NIH	https://imagej.net/software/imagej/
Imaris 8.3	Imaris	RRID:SCR_007370
WormLab	MBF Bioscience	N/A
Zen3.1	Zeiss	RRID:SCR_021725
Adobe Illustrator 2021	Adobe	RRID:SCR_010279
Code for analyzing the average speed	This paper	https://github.com/lingling-ll/Analyzing-speed-of-C.elegans.git
Other		
Leica TCS SP8 Confocal Microscope	Leica	N/A
Zeiss LSM980 NLO confocal microscope with Airyscan2	Zeiss	N/A
Spinning-disk confocal microscope	Olympus	N/A
DeltaVisonTM ultra microscope	Olympus	N/A
CFX96-qPCR	Bio-Rad	N/A
Leica EM UC7	Leica	N/A
Hitachi HT-9900 TEM microscope	Hitachi	N/A

RESOURCE AVAILABILITY

Lead contact

Further information and requests for resources and reagents should be directed to and will be fulfilled by the lead contact, Yu Chung Tse (tseyc@sustech.edu.cn).

Materials availability

Requests for strains should be directed to and will be fulfilled by the lead contact, Yu Chung Tse (tseyc@sustech.edu.cn).

Data and code availability

- All data reported in this paper will be shared by the lead contact upon request.
- All original code is available at: https://github.com/lingling-ll/Analyzing-speed-of-C.elegans.git.
- Any additional information required to reanalyze the data reported in this paper is available from the lead contact upon request.

EXPERIMENTAL MODEL AND STUDY PARTICIPANT DETAILS

C. elegans strains

All *C. elegans* strains were grown at 22°C on Nematode Growth Medium (NGM) plates seeded with *Escherichia coli strain OP50*. All strains used in this study are listed in Table S1.

Transgenic strain construction

The transgenic strains of endogenous *rsu-1(D108K;Y133K)* and mCherry::RSU-1(D108K;Y133K) were generated by SunyBiotech Company [strain name and genotype: PHX2149 rsu-1(syb1901 syb2149); PHX3846 rsu-1(syb1901 syb3846)]. The sequencing primers are listed in Table S2.

METHOD DETAILS

RNAi

We performed RNAi experiments using the method previously described.[37] To construct the *rsu-1(RNAi)* strain, we inserted its DNA fragment into the L4440 vector and transformed it into HT115 competent cells. The HT115 bacteria with the RNAi plasmid were then seeded on RNAi plates (NGM plates with 100 μg/ml ampicillin and 1 mM IPTG). For *rsu-1(RNAi)*, we hatched the embryos on the RNAi plates and then transferred L4 worms to a new RNAi plate for 24 hours before microscopy imaging.

Age synchronization and behavioral assays

For the locomotion assay, we placed 20-30 gravid adults on L4440(RNAi) plates or *rsu-1(RNAi)* plates. Once their progeny reached the L4 stage, we transferred them onto Amp/FUdR plates containing 49.5 μM Fluorodeoxyuridine and 100 μg/ml ampicillin. Then, these worms were considered as Day 1 adults.[38] Then, we transferred the Day 1 adults to the fresh NGM plates and immediately recorded their spontaneous movement for 1 minute using the Olympus MVX10 MacroView upright microscope equipped with the Olympus cellSens Standard software.[39] After recording, we transferred the Day 1 adult worms back to the fresh Amp/FUdR plates for further experiments. We repeated the process to acquire movement videos of Day 1, 5, and 10 adult worms. The locomotion speed of the worms was quantified using WormLab software (MBF Bioscience, Williston, VT). The final average speed was analyzed using a program, which can be found in the supplementary code. Initially, we collected the speed data for each time frame, totaling 423 frames, which included both forward (positive values) and reverse speeds (negative values). We first eliminated worms with a negative average speed and those with less than 100 recorded frames. Next, we removed any columns with more than 3 consecutive negative blocks and checked if the remaining columns had more than 100 frames. If they did, we calculated the average speed. If not, the worm sample was discarded.

Pluronic-based burrowing assay: 28 g Pluronic F-127 (Beyotime) was dissolved in 100 mL deionized water to reach the 28% w/v concentration (optimized protocol).[40] This solution was dissolved at 40°C for 20 min and kept at 12°C until totally dissolved and stored at 12°C before experiments. The burrowing assay was conducted in the 12-well plate, with three replicates tested in one group. 20 μL PF-127 was dripped at the bottom of well, and we picked 35 worms into the drop and then waited for 5 min at RT to make the drop solidified. Then we added 2.8 mL PF-127 gel and keep it at RT for 15min until we can use the worm picker to touch the gel surface. We picked L4440 RNAi bacteria pellet on the center of surface as the chemoattractant for the experiment. Then we count the number of worms on the agar surface every 15 mins. Animals for the burrowing assays are Day 1, 5, and 10 adults cultured in the Amp/FUdR plates.

For the aging worms in Figure S3, synchronized L4 stages worms were picked to fresh NGM plated seeded with OP50 every day to acquire the Day 1, 5, 10 and 15 adults.

Fluorescence microscopy

Staining the actin filaments of Day 1, 5, and 10 adults with Rhodamine Phalloidin (Abcam, ab235138) was carried out as previously described.[17]

For immunostaining of the thick filament in body-wall muscle. The protocol was referred to the Constant Spring Fixation method described by Wilson.[41] The primary antibody used in this study was anti-MHC A at 1:200 (DSHB, mouse monoclonal 5-6) and secondary antibody was goat anti-mouse IgG-Alexa Fluor™ Plus 647 at 1:200 (ThermoFisher A32728TR).

For live imaging, samples were anesthetized with 3% (-)-tetramisole on a 5% agarose pad and then turned over to the ventrolateral position to observe at least one bundle of muscle. To obtain 3D images of the dense body, z-stack images were acquired using a Leica TCS SP8 Confocal Microscope with a lightning super-resolution system equipped with a 63X oil /1.4 NA objective lens and Hybrid Detector (HyD), or a Zeiss LSM980 NLO confocal microscope with Airyscan2 equipped with a 63X oil /1.4 NA objective lens and GaAsP array PMT detector. For body wall structure including dense body, M-lines, phalloidin staining, and myosin filaments, inverted spinning-disk confocal microscopes were used, such as Olympus with Yokogawa CSU-X1 system equipped with a 60X oil /1.4 NA objective and CCD camera, Carl Zeiss LSM980

with Airyscan Confocal Microscope equipped with a 40X oil /1.3 NA objective and GaAsP array PMT detector, or DeltaVisonTM ultra microscope equipped with a 60X oil /1.4 NA objective and CCD camera. Images were acquired using ZEN 3.1 (blue edition), LAS AF, MetaMorph, and softWoRx software, respectively, and processed by Image J.

Quantitative PCR

The RT-PCR protocol was modified from the rapid RNA analysis of individual worm methods.[42] Ten worms were picked into 10 μL of worm lysis buffer (5 mM Tris pH 8.0, 0.5% Triton X-100, 0.5% Tween 20, 0.25 mM EDTA, and 1 mg/mL proteinase K), followed by incubation at 65°C for 10 min and then at 85°C for 1 min. gDNA eraser and cDNA synthesis were performed using the HiScript III 1st Strand cDNA Synthesis Kit (+gDNA wiper) (Vazyme). Quantitative PCR was carried out using SYBR Green Master Mix with the following program: 95°C for 30 s and 40 cycles of 95°C for 10 s, 60°C for 30 s, 95°C for 15 s, and 60°C for 60 s. All data were normalized to the tba-1 gene.

Transmission electron microscopy

The Day 10 adult worms grown on Amp/FUdR plates were washed with M9 buffer and then fixed with primary fixative (0.5% glutaraldehyde and 1.5% paraformaldehyde in 50 nM cacodylate buffer) at room temperature for 4 hr and washed with 50 nM cacodylate buffer. Samples were then postfixed in 2% OsO_4 in 50 nM cacodylate buffer at room temperature for 4 hr and then washed with ddH2O. Samples were dehydrated in an acetone series (20 min each in 25%, 50%, and 75%, 30 min for 90%, 30 min twice for 100%, and 100% overnight at 4°C), and then embedded in a spur resin series (90 min each in 25%, 50%, 75%, and 100%, 100% overnight at room temperature, and 100% at 60°C for 2 days).[17] The embedded samples were then sectioned into ultra-thin sections (~70 nm) using a Leica EM UC7. Ultra-thin sections were stained with 2% uranyl acetate and 3% lead citrate solution. Finally, sections were examined on a Hitachi HT-9900 TEM microscope.

QUANTIFICATION AND STATISTICAL ANALYSIS

For RSU-1 and UNC-97 expression in the whole worm (Figure 1A), z-stack images (interval - 0.15 μm) were acquired with the Tile function of Zeiss LSM980 NLO confocal microscope equipped with a 63X oil /1.4 NA objective and GaAsP array PMT detector.

For images of the dense bodies and M-lines, z-stack images (interval - 0.17 μm) were acquired by the Airyscan of Zeiss LSM980 NLO confocal microscope equipped with a 63X oil /1.4 NA objective. The images were set in the same threshold for the colocalization assays in the same strain. The 3D simulated images of dense body were constructed by the Imaris software.

The statistical significance of differences between different samples was compared by the unpaired two-tailed Student's t-test in GraphPad Prism.